

See discussions, stats, and author profiles for this publication at: <https://www.researchgate.net/publication/383427615>

Harnessing Radio-Frequency Energy Harvesting for Battery-Free Wireless Sensing

Preprint · August 2024

DOI: 10.13140/RG.2.2.12436.51842

CITATIONS

0

READS

71

8 authors, including:



Tao Ni

City University of Hong Kong

16 PUBLICATIONS 92 CITATIONS

[SEE PROFILE](#)



Zehua Sun

City University of Hong Kong

11 PUBLICATIONS 469 CITATIONS

[SEE PROFILE](#)



Mingda Han

Shandong University

7 PUBLICATIONS 13 CITATIONS

[SEE PROFILE](#)



Tao Gu

RMIT University

179 PUBLICATIONS 8,924 CITATIONS

[SEE PROFILE](#)

Harnessing Radio-Frequency Energy Harvesting for Battery-Free Wireless Sensing

Tao Ni*, Zehua Sun*, Mingda Han†, Guohao Lan‡, Yaxiong Xie¶, Zhenjiang Li*, Tao Gu||, Weitao Xu*

*City University of Hong Kong, †Shandong University, ‡Delft University of Technology,
¶University at Buffalo, SUNY, ||Macquarie University

ABSTRACT

Diverse Wi-Fi-based wireless applications have been proposed, ranging from daily activity recognition to vital sign monitoring. Despite their remarkable sensing accuracy, the high energy consumption and the requirement for customized hardware modification hinder the wide deployment of the existing sensing solutions. In this paper, we propose REHSENSE, an energy-efficient wireless sensing solution based on Radio-Frequency (RF) energy harvesting. Instead of relying on a power-hungry Wi-Fi receiver, REHSENSE leverages an RF energy harvester as the sensor and utilizes the voltage signals harvested from the ambient Wi-Fi signals to enable simultaneous context sensing and energy harvesting. We design and implement REHSENSE using a commercial-off-the-shelf (COTS) RF energy harvester. Extensive evaluation of three fine-grained wireless sensing tasks (*i.e.*, respiration monitoring, human activity, and hand gesture recognition) shows that REHSENSE can achieve comparable sensing accuracy with conventional Wi-Fi-based solutions while adapting to different sensing environments, reducing the power consumption by 98.7% and harvesting up to 4.5 mW of power from RF energy.

1 INTRODUCTION

Wi-Fi based wireless sensing systems are on the rise, with examples including health surveillance [1–3], activity recognition [4, 5], and gesture recognition [6–8]. Among the existing systems, Channel State Information (CSI) based design has attracted great attention due to its promise in achieving fine-grained context sensing and compatibility with Commercial-Off-The-Shelf (COTS) Wi-Fi devices. However, in the existing Wi-Fi CSI-based sensing works¹, we find that there are two practical limitations that hinder the wide adoption of Wi-Fi CSI-based sensing solutions.

(I) Customized hardware modification. First, existing CSI-based sensing systems utilize the Wi-Fi Network Interface Controller (NIC) card to receive the packets from the target Wi-Fi transmitter and leverage the CSI tool [9, 10] to extract the wireless channel information from the NIC. However, not all NIC cards support CSI extraction. In fact, most of the NIC manufacturers do not provide the access to CSI information. As a result, we can only leverage a very limited range of NIC cards to obtain the CSI data for sensing, *i.e.*, the Intel 5300 card [9] and the Qualcomm Atheros Wi-Fi chipset [10]. As shown in Figure 1a, our literature survey indicates that 74% of the investigated CSI-based sensing works utilize the Intel 5300 card [9], and 22% of them use the Qualcomm Atheros Wi-Fi chipset [10].

Moreover, since most of the CSI-extractable NIC cards are no longer adopted by the latest Wi-Fi devices, existing solutions have

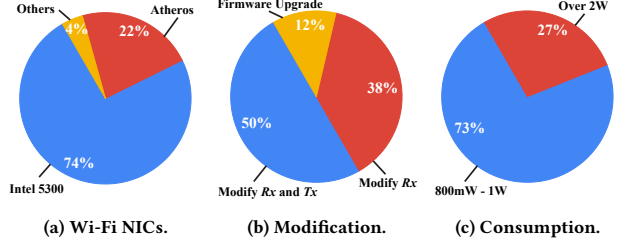


Figure 1: Literature survey on 50 representative CSI-based sensing works: (a) Wi-Fi NICs in investigated works; (b) Required hardware modifications; and (c) power consumption of 11 Wi-Fi NICs.

to compromise the device. This is done by replacing the original onboard NIC card in the device with a CSI-extractable alternate, which is not only impractical but also requires additional effort from the end users. As shown in Figure 1b, 50% of the existing works need to modify both of the transceivers (Wi-Fi NICs in both router and mobile device), 38% of them need to modify the receiver, and the remaining 12% of them require a firmware upgrade.

(II) High power consumption. The second limitation of existing Wi-Fi CSI-based works is the high power consumption of the NICs. Specifically, we investigate the power consumption of 11 CSI-extractable Wi-Fi NIC cards that are widely used by existing works². Their power consumption is briefly summarized in Figure 1c. Eight (73%) of them consume approximately 800 mW to 1 W when running in the idle receiver mode [11, 12]. Three of them (27%), *i.e.*, the three Intel Wi-Fi NICs, consume over 2 W to extract CSI information [13]. Due to the high power consumption, deploying Wi-Fi CSI-based sensing solutions on power-constrained devices, such as battery-powered IoT devices, becomes extremely difficult in a sustainable smart home.

To move beyond the current limitations and towards battery-free sensing, we present REHSENSE, a novel wireless sensing system based on RF Energy Harvesting. Specifically, RF energy harvesting is a passive power scavenging technique that converts ambient RF energy emitted from mobile devices, such as Wi-Fi routers and cellular towers, into direct current (DC) voltage signals that can be used to power electrical components and devices. It has been widely used in diverse commodity IoT devices, such as LED lights [14], tiny cameras [15], and self-sustaining sensors [16].

Key insights. Our key observation is that human activity significantly affects the amount of energy that the harvester harvests from the ambient RF signals, since the signal reflecting off the human body may superimpose constructively or deconstructively with multipath signals in the propagation environment at the harvester,

¹Complete list is available at: <https://github.com/REHSense/REHSense>

²Including the Intel 5300, three Intel AX200 Wi-Fi 6 series cards, and seven Qualcomm Atheros Wi-Fi chipsets.

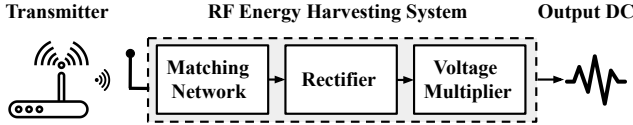


Figure 2: Workflow of RF energy harvesting.

depending on the position and pose of the human. Therefore, instead of purely utilizing it as a humdrum energy source, we propose to leverage the RF energy harvester as a novel battery-free activity sensor. Specifically, we measure the time-varying harvested power (voltage) as the sensing signal and apply a deep neural network to recognize human activities. We note that the relationship between the harvested energy and human activities has also been noticed in prior works [17, 18]. However, we take the first step towards building battery-free Wi-Fi based sensing systems using purely low-cost off-the-shelf commercial hardware.

We design and implement REHSENSE by using low-cost commercial hardware, *i.e.*, a Powercast P21XXCSR-EVB power harvesting board [19] and an Arduino Nano microcontroller. We evaluate REHSENSE’s performance with data collected from ten participants with four different COTS Wi-Fi routers in four typical environments (*i.e.*, home, office, corridor, and cafe). Extensive experimental results show that REHSENSE achieves an accuracy of 95.4%, 95.7%, and 90.8% in respiration monitoring, human activity recognition, and hand gesture recognition, respectively. Furthermore, we conducted an experiment to compare the sensing accuracy and energy consumption of our energy-efficient solution with that of conventional sensing solutions using Wi-Fi NIC. The results show that REHSENSE achieves a competitive sensing ability while consuming much lower energy than the CSI-based system. In addition, we present examples to demonstrate that REHSENSE can be integrated into different commodity IoT devices and provide a battery-free sensing prototype system based on RF energy harvesting.

Contributions. We summarize the following contributions.

- To the best of our knowledge, REHSENSE is the *first* practical energy-efficient Wi-Fi sensing solution, which opens the door for designing battery-free wireless sensing systems. To provide a solid basis for future work, we also propose a theoretical model for describing RF energy transmission in the presence of various human activities in the Fresnel diffraction zones.
- To support simultaneous energy harvesting and activity sensing, we design a lightweight pipeline of REHSENSE that consists of the hardware platform, signal processing modules, counting algorithms, and CNN-based neural networks. REHSENSE reduces the energy consumption of wireless sensing systems by orders of magnitude while imposing no hardware and firmware modifications to the existing Wi-Fi infrastructure.
- We design and implement a prototype of REHSENSE using COTS hardware circuits. Our extensive experimental results demonstrate that REHSENSE achieves high accuracy in monitoring respiratory rate, recognizing fine-grained human activities, and hand gestures. Moreover, in a comparison experiment with a conventional CSI-based sensing system, REHSENSE achieves competitive recognition accuracy in the same scenarios while consuming significantly lower energy.

2 PRELIMINARY

2.1 Primer on RF Energy Harvesting

RF energy harvesting is a passive power scavenging technique that converts ambient RF energy emitted by high electromagnetic fields, such as Wi-Fi routers and cellular towers, into direct current (DC) that can be used to power sensors and prolong battery life. As an example, Figure 2 shows a typical workflow of an RF energy harvesting system. The wireless transmitter (*e.g.*, a Wi-Fi router) radiates electromagnetic energy to the near-field space [20]. The receiving antenna captures the RF signal and feeds it into an impedance-matching network that maximizes energy harvesting efficiency. Then, a rectifier and a voltage multiplier are used to convert the harvested RF signal into DC voltage. Theoretically, the transmission of RF energy in free space follows the Friis’ transmission equation [21] as follows:

$$P_r = P_t \frac{G_r G_t \lambda^2}{(4\pi d)^2}, \quad (1)$$

where P_t , P_r are the transmitted power and the received power; G_t , G_r are the gains of the transmitting (Wi-Fi router) and the receiving (harvesting device) antennas; λ is the wavelength; and d is the distance between the two antennas. We can further obtain the gain of free-space RF energy transmission $Gain_{Friis}$ as:

$$Gain_{Friis} [dB] = 10 \log\left(\frac{P_r}{P_t}\right) = 10 \log\left(\frac{G_t G_r \lambda^2}{(4\pi d)^2}\right), \quad (2)$$

which describes the Line-of-Sight (LoS) harvested RF energy at distance d between the transmitter and the receiver.

2.2 Modeling Harvested Energy

The Fresnel zone diffraction model has been widely used in the analysis of fine-grained activity recognition [4, 22]. The key insight is that when a target is located inside the Fresnel zones, diffraction dominates and becomes much stronger than other propagation effects (*e.g.*, reflection and scattering). Prior studies [23] [24] have proved that more than 70% of the RF energy is transmitted in the First Fresnel Zone (FFZ). Thus, we leverage the Fresnel zone diffraction model to study the RF energy harvesting voltage signal.

Diffraction model formulation. We first define the boundary of the n th Fresnel zone as:

$$|TxP_n| + |RxP_n| - |TxRx| = \frac{n\lambda}{2}, \quad (3)$$

where the Wi-Fi router (Tx) and the RF energy harvesting device (Rx) are the foci of concentric ellipses and represent the Fresnel zones, P_n is the sensing target located at the boundary of the n th Fresnel zone (*e.g.*, $n = 1$ represents the FFZ), and λ is the wavelength of the RF signal.

Figure 3 illustrates the diffraction model in the FFZ. We assume the length of the semi-minor axis of the FFZ is r_1 , and the sensing target is walking in the middle of Tx and Rx (*i.e.*, $d_1 = d/2$ and $r_1 = \sqrt{\lambda d_1}/2$). The distance from the front and back sides of the human body to the LoS of the transceivers is h_{front} and h_{back} , respectively. We can also obtain the Fresnel front clearance and the Fresnel back clearance as $u_{front} = h_{front}/r_1$ and $u_{back} = h_{back}/r_1$, respectively. Then, we obtain the Fresnel-Kirchhoff diffraction parameters $v_{front} = \sqrt{2}u_{front}$ and $v_{back} = \sqrt{2}u_{back}$ [4]. Finally, the

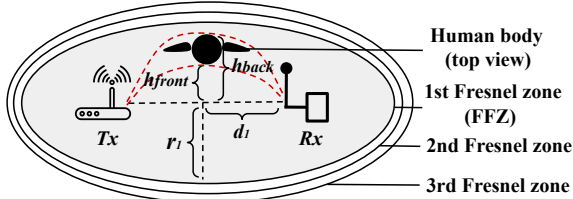


Figure 3: Illustration of the diffraction model in the FFZ.

amplitude of the RF signals captured by the RF energy harvesting device, which is subject to the diffraction of the front and back sides of the human body, can be expressed as:

$$\begin{aligned} F(v_{front}) &= \frac{1+j}{2} \int_{v_{front}}^{\infty} e^{\frac{-j\pi z^2}{2}} dz, \\ F(v_{back}) &= \frac{1+j}{2} \int_{-\infty}^{v_{back}} e^{\frac{-j\pi z^2}{2}} dz, \end{aligned} \quad (4)$$

where $e^{-j\pi z^2/2}$ is the phase shift in the diffraction path z . When a human body is inside the FFZ, the total diffraction gain is the sum of diffraction gains of the front and back sides, which is defined as:

$$Gain_{Diff} [dB] = 20\log |F(v_{front}) + F(v_{back})|, \quad (5)$$

which describes the increases of harvested RF energy caused by the human body's diffraction effect.

Modeling the harvested energy. So far, we have introduced the free-space gain of RF energy transmission $Gain_{Friis}$ and the gain of Fresnel diffraction $Gain_{Diff}$. In practice, however, there are many partitions and obstacles that can block the LoS RF energy transmission, and result in path losses. Thus, we further model the path loss at a distance d as follows:

$$\begin{aligned} PL(d) [dB] &= PL(d_0) + 10n\log\left(\frac{d}{d_0}\right) + FAF [dB] \\ &\quad + p * AF_{partition} [dB] + q * AF_{wall} [dB], \end{aligned} \quad (6)$$

where $PL(d_0)$ is the path loss at reference distance (typically, $d_0 = 1$ m), FAF is the floor attenuation, p and q are the number of soft partitions (*i.e.*, human body) and concrete walls, respectively, $AF_{partition}$ and AF_{wall} are the corresponding attenuation factors, respectively. In addition, path loss describes the decrease of harvested RF energy when the human body totally or partially blocks LoS RF signal transmissions.

In a nutshell, the energy generated by the RF energy harvesting device is the combination of the path losses $PL(d)$ and the two dominant gains, *i.e.*, $Gain_{Friis}$ and $Gain_{Diff}$. Thus, leveraging Equation 2, Equation 5 and Equation 6, we can model the harvested energy and use it to achieve fine-grained activity recognition without the need of the conventional power-hungry wireless receiver. As shown later in our system profiling (§ 4.5), the proposed RF energy harvesting-based wireless sensing consumes only 11.3–12.6 mW power, in contrast to the 820–940 mW power consumed by conventional Wi-Fi NIC card. Below, we conduct a preliminary study to investigate the feasibility of the proposed idea.

2.3 Feasibility Study

We conduct a preliminary study to demonstrate the feasibility of using energy harvesting for wireless sensing. In this study, we

consider three mainstream wireless sensing tasks: respiration monitoring, human activity recognition, and hand gesture recognition. For each sensing task, we monitor the voltage signals generated by an RF energy harvester when a subject is inside the FFZ between a commodity Wi-Fi router and an RF energy harvesting device (details of the hardware and setup are shown later in Figure 8).

- **Case study 1: Respiration monitoring (RM).** The three plots in Figure 4a are the normalized voltage signals when a participant is breathing normally in different positions, including lying, sitting, and standing. The harvested signals show the continuous rise and fall patterns that correspond to the subtle displacements of the subject's chest. Recall our modeling in the previous subsection, the subtle displacement leads to changes in the diffraction gain in the FFZ, as well as the harvested RF energy.

- **Case study 2: Human activity recognition (HAR).** Figure 4b shows the harvested voltage signals when the person is performing three daily activities: walk, push-up, and sit-up. The signal patterns can also be illustrated by the diffraction model in § 2.2. Taking walking as an example, when the person is approaching the FFZ, the diffraction gain increases, and hence more RF energy is captured by the receiver. Then, the person arrives in the middle of the FFZ, and the human body blocks the LoS energy transmission which increases the energy of path loss. Finally, as the person moves out of the FFZ, the harvested RF energy increases because the energy caused by path loss increases and the diffraction effect strengthens the harvested RF energy. Using the same principle, we can explain the patterns exhibited in the harvested signals of push-up and sit-up.

- **Case study 3: Hand gesture recognition (HGR).** Figure 4c shows the harvested RF energy signals of three hand gestures: waving hand, drawing a circle, and flipping the palm. We observe that different hand gestures lead to different bursts of captured RF energy because the moving hand changes the diffraction gain in the FFZ. Therefore, it is feasible to recognize fine-grained hand gestures using RF energy harvesting.

The preliminary results from the three case studies above show that changes in harvested RF energy can reflect human activities and vital signals such as respiratory rate. Moreover, different human activities (*i.e.*, walking, push-ups, sit-ups) and human hand gestures inside the FFZ also present distinct RF energy patterns, demonstrating the feasibility of harnessing RF energy harvesting-based wireless sensing.

3 DESIGN AND IMPLEMENTATION

3.1 System Overview

Based on the proposed diffraction model and the results of the feasibility study, we present REHSENSE, a novel wireless sensing system via RF energy harvesting. REHSENSE implements a lightweight sensing pipeline that supports diverse sensing applications. We choose to implement three sensing tasks listed in our feasibility study for two reasons. First, they are the most representative applications in the wireless human sensing field [25]. Second, they cover different levels of granularity: respiration monitoring (minor movement), human activity recognition (large-scale movement), and hand gesture recognition (small-scale movement). Therefore, these

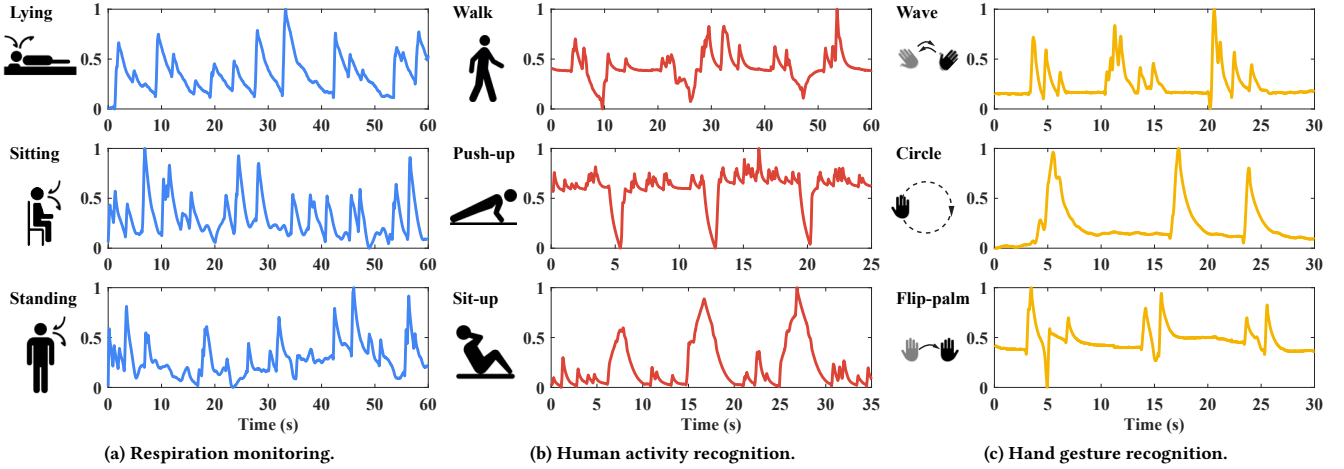


Figure 4: Feasibility study: harvested voltage signals (normalized) in three wireless sensing tasks.

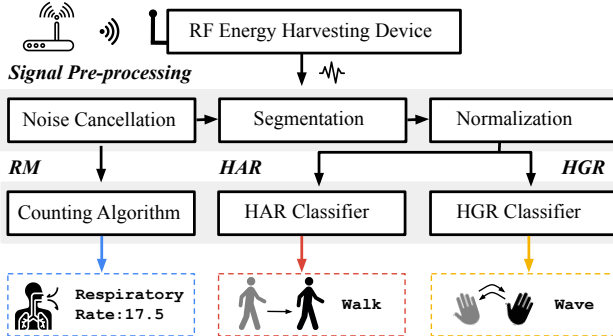


Figure 5: Overview of REHSENSE.

three sensing tasks can demonstrate the potential of REHSENSE in enabling various applications for wireless sensing tasks.

Figure 5 depicts the system overview of REHSENSE, which consists of three components. First, the RF energy harvesting device captures the RF signals sent by the Wi-Fi router and converts the RF signals to DC output (time-series voltages). Second, the signal pre-processing module performs noise cancellation to remove interference, segmentation to obtain segments containing activities and gestures, and normalization to generate valid input for training or recognition. Then, the counting algorithm takes the filtered voltage signal and outputs the calculated respiratory rate to achieve respiration monitoring (RM). The pre-trained CNN-based HAR and HGR classifiers can predict the activities and gestures from the normalized signal segments, respectively.

3.2 Signal Pre-processing

Noise cancellation. The harvested voltage signal contains noise that results from other transmitter sources and ambient interference. In REHSENSE, we apply a Savitzky-Golay (S-G) filter [26] for noise filtering. S-G filter fits successive slices of signal with a low degree polynomial function to maintain the time and frequency domain patterns of the time-series signal [27]. Thus, it can effectively remove both high-frequency noise and small variations in the harvested signal caused by interference from other transmitters.

Signal segmentation. We utilize a variance-based sliding window (*i.e.*, 0.5 s with a 50% overlapping rate) to divide the time-series voltage signal into segments. Specifically, the variance-based sliding window finds the segmentation points where the variance is lower than a pre-defined threshold (*i.e.*, 0.1 in our current design). The threshold is selected when no activity movements are performed, and the corresponding harvested voltage signal remains constant.

Normalization. According to Equation 1, the distance between the two antennas affects the strength of the harvested RF energy. To reduce its impact on activity and gesture recognition, we normalize the signal segments to the range of [0, 1] by deducting the DC offset (average voltage where variance is less than 0.01). In addition, the length of activity/gesture segments is different, so we apply the down-sampling method to resize the segments with different lengths to 1×128 vectors as valid input of the CNN neural network in both training and testing processes.

3.3 Respiration Monitoring (RM)

In § 2.3, we present that the RF signals of human respiration exhibit periodic motions that correspond to the rise and fall of the chest. However, we also find that some voltage spikes overlap together as the respiratory rate can be fast, and hence the harvested RF energy is a combination of the neighbor respiration. To address this overlap issue and achieve accurate respiration monitoring, we propose a *variance-peak* counting algorithm (see Algorithm 1) that can calculate the respiratory rate by a moving-variance window and peak analysis. Specifically, it first obtains the variance signal by applying a moving-variance sliding window (Line 2 – 5) and then finds peaks in the variance signal and uses the number of peaks to calculate the final respiratory rate (Line 6 – 7). In REHSENSE, we set the size of the moving-variance window as 100 with a given variance threshold as 0.002, and use the peak analysis function provided by the Signal Processing Toolbox of MATLAB (R2022a).

Figure 6 presents an example of applying the *variance-peak* counting algorithm to calculate the respiration rate when a person is lying down on a mat. The upper figure shows the original harvested voltage signal and the lower figure presents the results after applying the proposed algorithm. It can be seen that compared to the original noisy signal in the upper figure, the peaks which

Algorithm 1: Variance-Peak Counting Algorithm

Input: \mathcal{S} : filtered harvested voltage signal.
 w : moving-variance window size.
 τ : given variance threshold.

Output: r : calculated respiratory rate.

```

1  $\mathcal{V} \leftarrow \mathcal{V}_0, \mathcal{V}_0 = \phi$  {initialize an empty variance array}
2 for  $i = 0; i < \text{len}(\mathcal{S}) - w + 1; i = i + 1$  do
3    $\mathcal{V}_i = \text{variance}(\mathcal{S}_i, \mathcal{S}_{i+w})$  {variance of a window}
4   if  $\mathcal{V}_i \geq \tau$  then
5      $\mathcal{V} \leftarrow \mathcal{V}_i$  {append  $\mathcal{V}_i$  to  $\mathcal{V}$ }
6  $\mathcal{P} = \text{findpeaks}(\mathcal{V})$  {find peaks in variance signal}
7 Output respiratory rate  $r$  with  $r = N_{\mathcal{P}}/t_{\mathcal{S}}$  { $N_{\mathcal{P}}$  is the number of peaks and  $t_{\mathcal{S}}$  is the time duration.}

```

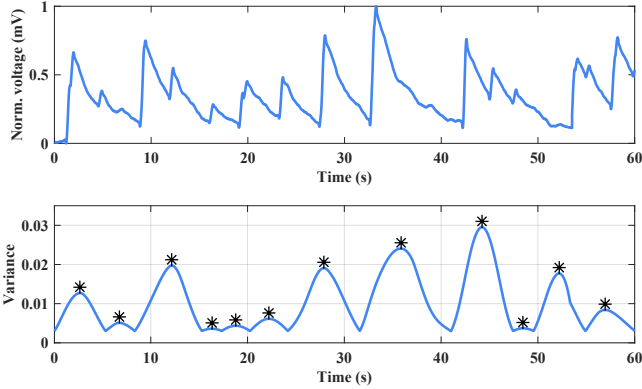


Figure 6: An example showing the performance of the variance-peak respiration counting algorithm. The number of black asterisks denotes the number of respiration during the monitoring period.

correspond to breathing rate can be easily spotted in the lower figure after using our algorithm.

3.4 Human Activity and Hand Gesture Recognition (HAR and HGR)

To determine the type of human activity or hand gesture, we apply a Convolutional Neural Network (CNN) method to achieve activity and gesture classification in REHSENSE. Because CNN-based neural network supports classic classification models that can extract both temporal and spatial features from the harvested voltage signals while achieving high accuracy in class prediction. Figure 7 shows the architecture of the proposed CNN neural network that consists of six layers: three convolutional layers for extracting temporal and spatial features from the one-dimensional signal segments, two fully connected layers that take the extracted feature vectors to generalize the neural network and learn the non-linear combinations of these features. At last, a softmax function is utilized in the classifier to output the predicted activity/gesture type.

Specifically, each convolution layer uses ReLU as the activation function and is followed by a max pooling layer with a pool size of 2. A flatten layer is used to convert the feature map to a one-dimensional feature vector, fed into the fully-connected layer. A dropout layer is used after the first fully-connected layer to avoid over-fitting, and the dropout rate is set to 0.5. We implement the

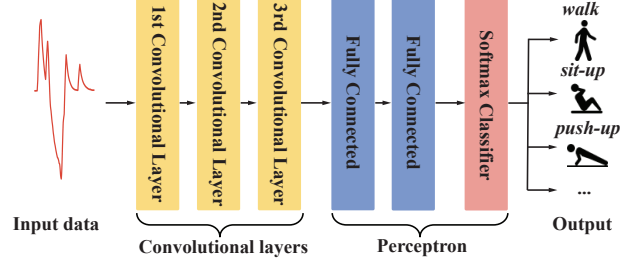
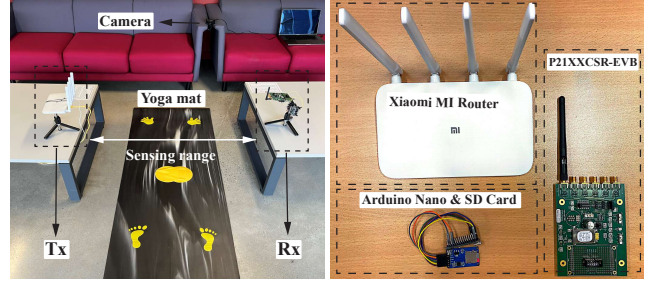


Figure 7: Architecture of the CNN neural network.



(a) Experimental setup.

(b) Hardware devices.

proposed CNN model in Keras 2.3 on the Tensorflow 2.0 framework and train 300 epochs in total with an initial learning rate of 0.01.

4 EVALUATION

4.1 Experimental Setup

Figure 8 shows the experimental environment, setup, and the hardware devices used in the experiments. We use a Xiaomi MI Router as the transmitter (Tx) and implement a prototype of RF energy harvesting as the receiver (Rx). In the prototype, we use an RF energy harvesting evaluation board, Powercast P21XXCSR-EVB [19], with one 2.4 GHz, and one 2.3 dBi dipole antennas to harvest RF energy from. To record the harvested voltage data, we use an Arduino Nano microcontroller and a 32 GB MicroSD card as the data recorder. The sampling rate of the data recorder is 200 Hz. We consider the experiments in an indoor scenario (e.g., room 5.7 m \times 4.2 m) and set the sensing range between Tx and Rx to 1.0 m and the height of Tx and Rx to 0.5 m. We also place a camera to record the experimental process, which will be used as a reference to analyze the results. All data processing and model training are conducted on a desktop running Windows 10 with 32 GB memory and an Intel i7-9700K CPU and an NVIDIA GeForce RTX 2080Ti GPU. In addition, we conduct experiments to explore the performance of REHSENSE in different settings (i.e. Wi-Fi routers, sensing ranges, environments) in § 4.4.

4.2 Dataset

We recruit ten participants³ to collect three independent datasets for three different sensing tasks: respiration monitoring dataset \mathcal{D}_{RM} , human activity recognition dataset \mathcal{D}_{HAR} , and hand gesture recognition dataset \mathcal{D}_{HGR} . The details are illustrated below.

- \mathcal{D}_{RM} : We ask the participants to breathe naturally in three common conditions: lying, sitting, and standing. For each participant, we record the harvested voltage signal in one minute and repeat

³This work has been approved by the IRB board of our institution.

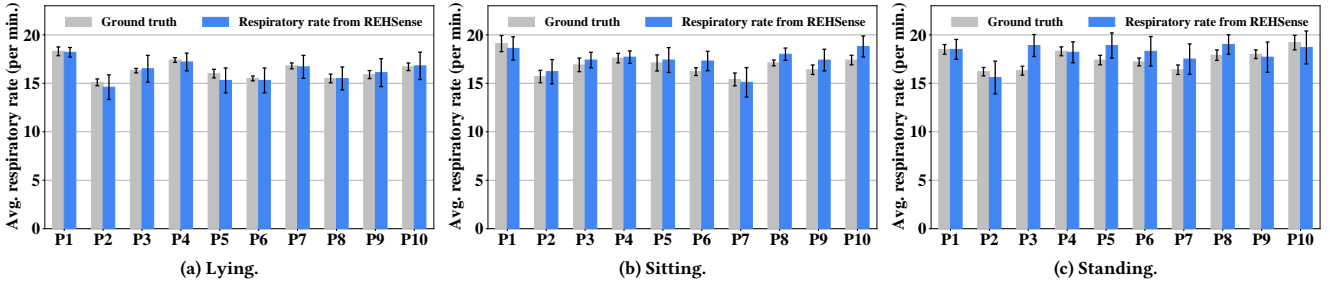


Figure 9: Effectiveness of respiration monitoring in three situations.

	walk	sit-up	push-up	high knee	leg lift	lunge	plank hold	squat	crunchy	sit-down	
walk	1	0	0	0	0	0	0	0	0	0	circle
sit-up	0	0.9	0.02	0	0	0.04	0	0.02	0	0.02	flap
push-up	0	0	1	0	0	0	0	0	0	0	flip-palm
high knee	0	0	0	1	0	0	0	0	0	0	front-back
leg lift	0	0	0	0	1	0	0	0	0	0	slide
lunge	0.07	0	0	0	0	0.86	0	0	0.07	0	square
plank hold	0	0	0	0	0	0	1	0	0	0	triangle
squat	0	0	0	0.03	0	0.02	0	0.92	0	0.03	up-down
crunchy	0	0	0	0	0	0	0.02	0.04	0.94	0	wave
sit-down	0	0	0	0	0	0	0	0	0.05	0.95	zig-zag
HAR results.											
	circle	flap	flip-palm	front-back	slide	square	triangle	up-down	wave	zig-zag	
circle	0.94	0	0	0	0	0	0	0.02	0	0.04	
flap	0.05	0.9	0	0	0	0	0	0.05	0	0	
flip-palm	0	0	0.92	0	0.05	0	0	0	0.03	0	
front-back	0.01	0.01	0	0.95	0	0	0	0.02	0	0.01	
slide	0	0	0.02	0	0.89	0.06	0.01	0	0.02	0	
square	0	0	0	0	0	0.9	0.08	0.01	0	0.01	
triangle	0	0.01	0	0	0.04	0.07	0.87	0.01	0	0	
up-down	0.02	0.02	0	0.01	0	0	0	0.95	0	0	
wave	0	0	0.04	0	0.01	0	0	0	0	0.92	0.03
zig-zag	0	0.03	0	0.03	0	0	0	0.06	0.03	0.85	
HGR results.											

Figure 10: Confusion matrices of the classification results of ten human activities (HAR) and ten hand gestures (HGR).

this process for ten times ($3 \times 10 \times 10 = 300$ minutes respiration data in total). To obtain the ground truth, each participant wears a commercial wearable device FLOWTIME headband [28] during the data collection.

- \mathcal{D}_{HAR} : We ask the participants to perform ten different exercise activities including walk, sit-up, push-up, high knee, leg lift, lunge, plank hold, squat, crunchy, and sit down. Each participant is asked to perform 10 groups of each activity with five repetitions ($10 \times 10 \times 10 \times 5 = 5000$ samples in total). In the evaluation, 80% of the dataset is randomly selected to train the activity recognition classifier while the rest of 20% data is used for testing.
- \mathcal{D}_{HGR} : We ask the participants to perform ten different hand gestures including slide, front-back, up-down, zig-zag, wave, circle, triangle, square, flap, and flip-palm. Each participant is asked to perform 10 groups of each gesture with five repetitions of both left-hand and right-hand ($10 \times 10 \times 10 \times 5 \times 2 = 10000$ samples in total). Similarly, we use 80% data samples to train the CNN neural network of the hand gesture classifier and evaluate the performance with the rest of 20% data samples.

4.3 Overall Effectiveness

Metrics. For respiration monitoring, we obtain the respiratory rate with the standard deviation (STD) of each participant and compare the respiratory rate produced by REHSENSE with the recorded ground truth. We use the classification accuracy and confusion matrix as metrics for human activity and hand gesture recognition.

Effectiveness of RM. Figure 9a, Figure 9b, and Figure 9c show the average respiratory rates of the ten participants from REHSENSE and their corresponding ground truths when the participants are lying,

sitting, and standing, respectively. Among all the ten participants, the calculated respiratory rate presents a maximum error of 4.6%, 6.4%, and 13.2% in three situations. The detection accuracy when the participant is lying (accuracy 95.4%) and sitting (93.6%) is higher than that of standing (accuracy 86.8%). This is because when the participant is standing, the rise-and-fall of both the front chest and the back causes diffraction effects, making respiration monitoring more challenging. In addition, we find the average respiratory rate provided by REHSENSE is close to the ground truth but REHSENSE's calculation presents a larger standard deviation (averagely STD 1.2%, ground truth STD: 0.59%) which means REHSENSE performs better when monitoring the respiration for a long-time duration.

Effectiveness of HAR. Figure 10a shows the classification results (confusion matrix) of the trained CNN-based HAR classifier. The overall accuracy in recognizing the ten involved human activities is 95.7%. From the result, we find that REHSENSE can accurately recognize activities like walk, push-up, and high knee (100% accuracy), but performs the worst in recognizing activities like sit-up (accuracy 90%) and lunge (accuracy 86%) because these activities requires the person to perform similar actions, i.e., bending knees to squat, which results in close patterns of the harvested voltage signals and increases the number of misclassified activities.

Effectiveness of HGR. Figure 10b shows the classification results (confusion matrix) of the trained CNN-based HGR classifier. The overall accuracy in recognizing the ten involved hand gestures is 90.8%. In addition, we observe REHSENSE performs the best in recognizing hand gestures such as front-back and up-down (accuracy 95%) but presents the lowest accuracy in recognizing gestures such as zig-zag (accuracy 85%) and triangle (accuracy 87%) because gestures like zig-zag and up-down, triangle and square have similar

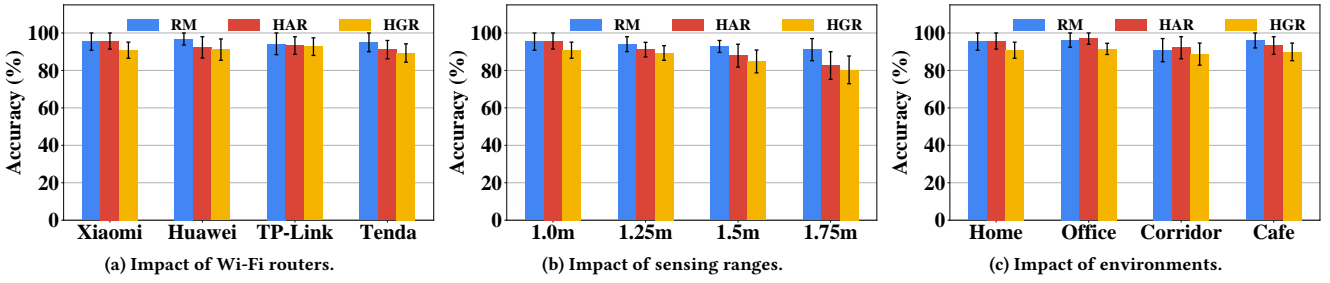


Figure 11: Analysis of the impact of different Wi-Fi routers, sensing ranges, and environments.

keystrokes and tracks, which causes similar energy patterns and increases the number of misclassified gestures.

4.4 Impact of Practical Factors

Different Wi-Fi routers. In § 4, we present the overall effectiveness of REHSENSE with the Xiaomi MI Router. To evaluate the impact of different commodity Wi-Fi routers and demonstrate the generalization ability of our system, we follow the same procedures in the aforementioned three sensing tasks with other three Wi-Fi routers: Huawei 4G Router 2 Pro, TP-Link TL-WR742N, and Tenda F3. Figure 11a shows the accuracy in calculating the respiratory rate (lying), determining human activities, and recognizing hand gestures of different Wi-Fi routers. For the three sensing tasks, the maximum differences in accuracy rates using different Wi-Fi routers are 2.6%, 4.6%, and 3.4%, respectively, demonstrating the robustness of REHSENSE for different Wi-Fi routers.

Different sensing ranges. As mentioned in § 2.1, the harvested RF energy depends on the distance (*a.k.a.* sensing range) of Tx and Rx . To investigate the impact of different sensing ranges, we adjust the sensing range from 1.0 m (default setting) to 1.25 m, 1.5 m, 1.75 m, and repeat the similar experiment processes. Figure 11b shows the classification accuracy of REHSENSE in different sensing tasks at different sensing ranges. We find the accuracy rates of the three sensing tasks decrease approximately by 4.3%, 13.1%, and 10.5% as the sensing range changes from 1.0 m to 1.75 m. This is because as the sensing range increases, the FFZ becomes larger and sensitive to the surrounding noise (*i.e.*, other transmitter sources, movements) that deteriorates the performance of REHSENSE. Moreover, the harvested energy decreases due to the transmission attenuation of RF signal, leading to a low signal-to-noise ratio. For example, when the Wi-Fi router and the RF energy harvesting device are separated by 1.2 m, nearly 90% energy is lost in the air [29]. Despite the sensing range in our current settings being limited (*e.g.*, <1.75 m), we present REHSENSE as a proof of concept that we can harness RF energy harvesting for wireless sensing. In practice, the sensing distance can be extended by implementing a more powerful energy harvester with high-gain antennas and more RF-DC converters. For instance, works such as [30] can harvest RF energy at a maximum distance of 9.75 m, and we will focus on extending the sensing distance of REHSENSE to make it more robust in our future work.

Different environments. We further conduct the same experiments in the other three common indoor scenarios (office, corridor, and cafe) to investigate the impact of environments. Figure 11c presents the classification accuracy of the three sensing tasks in different environments. In different environments, REHSENSE shows

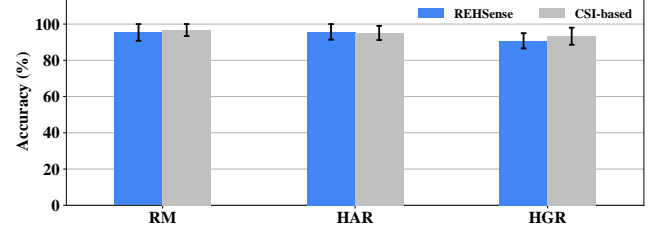


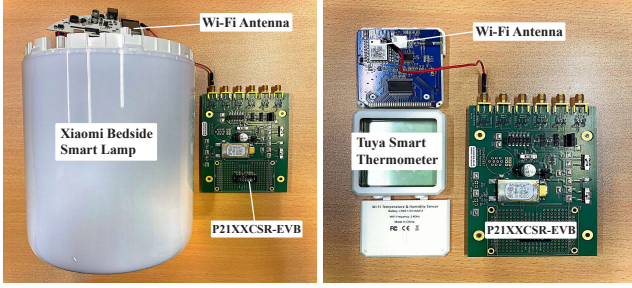
Figure 12: Comparison with the CSI-based sensing system.

overall accuracy rates of 94.6%, 94.5%, and 90.2% for respiration monitoring, activity recognition, and gesture recognition, respectively. We notice that the maximum accuracy difference in the four environments is 5.4%, 4.9%, and 2.8% only. This is because the small signal variations induced by the environment noise (*e.g.*, other people's movements) can be removed by the S-G filter as has been proved in previous studies [4, 24]. The results demonstrate the robustness of REHSENSE in different environments.

4.5 Comparison with Wi-Fi CSI-based Sensing

Sensing accuracy. We now compare the performance of REHSENSE with the state-of-the-art Wi-Fi CSI-based approaches in the same settings. For the hardware, we install the commonly used the Linux 802.11n CSI tool [9] on a Lenovo T400 laptop to extract CSI. Then, we implement the methods proposed by Zhang et al. [4], Gao et al. [6], and Zhang et al. [31] as the baseline of activity recognition, gesture recognition, and respiratory monitoring, respectively. Figure 12 compares the accuracy of REHSENSE with the corresponding CSI-based system in the three sensing tasks. Specifically, REHSENSE and the CSI-based sensing system separately achieve accuracy of 95.4% vs. 96.7% in respiration monitoring, 95.7% vs. 95.1% in human activity recognition, and 90.8% vs. 93.3% in hand gesture recognition. The result shows REHSENSE achieves comparable accuracy with the CSI-based systems.

Energy efficiency. To demonstrate the energy-efficient of our system, we use the Monsoon Power Monitor to measure the energy consumption of each hardware component. REHSENSE utilizes a passive RF energy harvesting board to capture Wi-Fi signal, which does not consume any energy. The Arduino Nano (with a MicroSD card) consumes 11.3–12.6 mW for data collection. By contrast, an Intel 5300 NIC card in the CSI-based sensing system consumes 820–940 mW [11, 12] to receive Wi-Fi packets. Hence, REHSENSE reduces around 98.7% energy consumption in the hardware. Moreover, the harvested RF energy is converted to DC voltages that can be used for charging sensors and batteries. For instance, assume an



(a) w/ Xiaomi bedside lamp. (b) w/ Tuya thermometer.

Figure 13: Integrate REHSENSE into IoT devices.

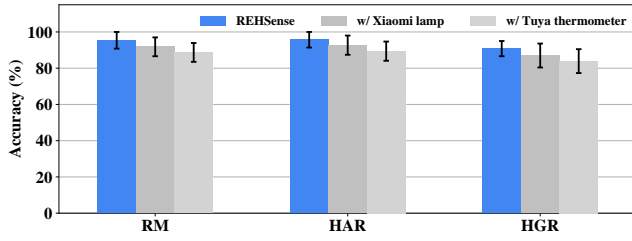


Figure 14: Effectiveness of integrating with IoT devices.

IoT device (*i.e.*, LED lamp) is powered by a 9 V, 550 mAh rechargeable battery that can support a power-intensive component like Intel 5300 NIC for only 5.3 – 6.0 hours, whereas the battery can support the low-power REHSENSE for around 400 hours. In addition, REHSENSE can harvest approximate 4.5 mW RF energy at the distance of 1 m for charging the battery so that it can prolong the usage and lifestyle of this IoT device.

4.6 Integrating REHSENSE into IoT Devices

In this experiment, we present examples of integrating REHSENSE into commodity IoT devices to demonstrate the feasibility and usability of REHSENSE. Figure 13 shows that we integrate the REHSENSE into a Xiaomi bedside smart lamp and Tuya smart thermometer by connecting its on-chip Wi-Fi antenna to the RF energy harvesting board. Then, we use these two modified IoT devices as the receiver to evaluate the performance of REHSENSE in the three wireless sensing tasks. Figure 14 presents the results of using the Xiaomi bedside smart lamp and Tuya smart thermometer as the wireless receiver (with the RF energy harvesting board), as well as the overall effectiveness we have shown in § 4.3. We can see that the REHSENSE-equipped Xiaomi bedside smart lamp shows accuracy rates of 91.8%, 92.7%, and 87.0% in respiration monitoring, human activity recognition, and hand gesture recognition, respectively. The modified Tuya smart thermometer shows 88.7%, 89.4%, and 83.9% accuracy in the three sensing tasks. Compared to the original REHSENSE prototype, the accuracy rates of the three sensing tasks drop approximately by 6%-7% as the inner antennas of commodity IoT devices are not powerful as an external antenna used in REHSENSE. Nevertheless, experiment results still show high feasibility and usability of REHSENSE in daily IoT devices.

4.7 Potential of Battery-free Sensing

Since REHSENSE has shown promising sensing performance and low power consumption, we then implement a prototype system to

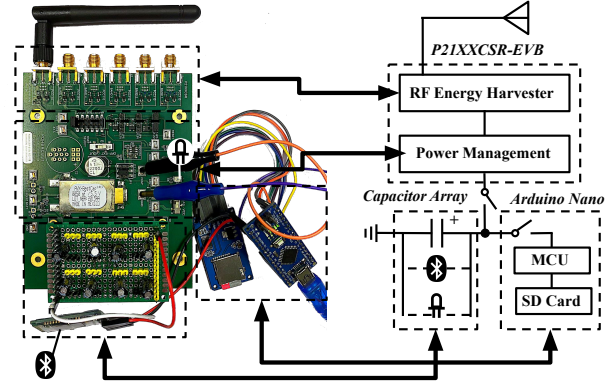


Figure 15: A prototype of the battery-free sensing system.

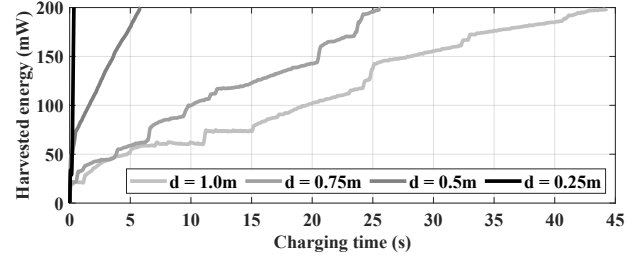


Figure 16: The harvested energy in the capacitor array vs. charging time at different distances.

demonstrate how REHSENSE pushes human sensing from power-hungry sensing to battery-free sensing. Figure 15 presents the prototype system as well as its circuit diagram, which consists of three components: an RF energy harvesting board (P21XXCSR-EVB), a storage capacitor array made by eight parallel 330 μ F capacitors, and an Arduino Nano MCU with a MicroSD card. Specifically, the capacitor array is designed for storing harvested energy and then using the storage to support electrical components [30, 32], while the Arduino Nano and MicroSD card record the DC voltages for different sensing tasks. Below, we provide two application examples of the prototype system to illustrate how to achieve battery-free sensing based on our prototype of REHSENSE.

Application 1: Sensing and Powering. In § 4.6, we present REHSENSE can be integrated into commodity IoT devices and achieve promising sensing accuracy. It also inspires us to think: *can we achieve battery-free sensing by using the harvested energy for sensing and powering simultaneously?* With this question, we further optimize the above prototype by adjusting the sensing range to obtain a high harvested voltage and then explore the possibility that the captured RF energy can be used for lighting a LED and sensing without any external power sources (*i.e.*, battery, USB powerline). Specifically, we utilize a B&K Precision 2190E 2-channel digital oscilloscope to monitor the changes in the harvested RF energy when the LED keeps lighting (harvested voltage ≥ 1.6 V). We find the oscilloscope shows distinctive patterns of different hand gestures at a sensing range of 10 cm while the harvested RF energy can also power the surface-mount LED module simultaneously. Even with a limited sensing range, this example shows that REHSENSE has the potential to achieve wireless sensing and power small IoT devices such as LED lights simultaneously, enabling various self-powered devices with wireless sensing capability.

Application 2: Sensing and Communication. Since we have demonstrated that the harvested energy can be used to support electrical components like LED modules, another question arises: *can we use the harvested RF energy to support communication so that we can transmit the harvested voltage data to the remote devices for different sensing tasks?* As the RF energy harvester can only store limited energy, we attach a capacitor array to store more harvested RF energy to achieve the application of supporting power-intensive components such as a Bluetooth module. Specifically, we use the Bluetooth module HC-05 that is running over a 3.3 V voltage with 200 mW power to support the communication, and it takes extra time to charge the capacitor array for storing enough power to achieve one data transmission process. We further explore the charging time with stored harvested RF energy at different sensing ranges from 1.0 m to 0.75 m, 0.5 m, 0.25 m and record the harvested RF energy in charging the external capacitor array so that it has enough energy to power the Bluetooth module. Figure 16 presents the time-voltage curves with different sensing ranges when the harvested RF energy is monitored for sensing and being used for charging the capacitor array. We find as the sensing range decreases, the charging time also decreases since much more Line-of-Sight RF energy is harvested by our devices. For instance, it takes 44.1 s, 25.6 s, 6.0 s, and 0.4 s to store enough energy to support one Bluetooth communication with sensing ranges of 1.0 m, 0.75 m, 0.5 m, and 0.25 m, respectively. The results reflect that a trade-off between the charging time and the sensing range should be considered to make REHSENSE in realizing battery-free sensing and communications.

The two experiments above demonstrate the potential of using RF energy harvesting to achieve ubiquitous battery-free sensing and corresponding applications, and REHSENSE makes the first step towards this goal.

4.8 Comparison with Other Sensing Techniques

To further illustrate the advantages of the proposed RF energy harvesting-based wireless sensing technique, we compare REHSENSE with four types of well-known sensing techniques: vision-based sensing [33, 34] (*i.e.*, camera-based), IMU-based sensing [35, 36] (*i.e.*, accelerometer, gyroscope), kinetic energy harvesting (KEH) based sensing [37, 38], and RFID-based backscatter sensing systems [39, 40]. Table 1 shows the comparison results from four metrics: (1) intrusive or non-intrusive sensing. (2) Coarse-grained or fine-grained recognition. (3) Active or passive sensing. (4) power-hungry or energy efficient.

Compared with vision-based sensing systems [33, 34] that use cameras to capture images and videos for human sensing, REHSENSE shows high efficiency in energy consumption since the RF energy harvester has no power consumption to monitor the power traces of the transmitting RF signals. IMU-based sensing systems [35, 36] are popular since most commodity mobile devices have equipped with IMU sensors (*i.e.*, accelerometer, gyroscope, and magnetometer). However, these IMU-based systems require the user to hold their smartphones or wear a smartwatch to intrusively obtain the data traces resulting from different human activities or hand gestures. To move a step to the concept of battery-free sensing, recent works [37, 38] proposed new techniques named kinetic energy harvesting (KEH) that convert kinetic energy to current traces, and

Table 1: Comparison with other four types of wearable/wireless sensing techniques. ● for “Yes”, ○ for “No”, ▷ for “Partially”.

Sensing system	Non-intrusive?	Fine-grained?	Passive?	Energy-efficient?
Vision-based [33, 34]	●	●	○	○
IMU-based [35, 36]	○	●	○	○
KEH-based [37, 38]	○	○	●	●
RFID-based [39, 40]	●	●	●	▷
REHSENSE	●	●	●	●

then use these traces for human sensing. Nevertheless, KEH-based sensing systems also require the user to wear specific sensors and can only recognize coarse-grained human activities [37]. Furthermore, RFID-based sensing systems [39, 40] seem to share the same principles of REHSENSE as passive RFID tags also integrated with RF energy harvesting circuits to scavenge the RF energy sent by the RFID reader. However, RFID-based sensing systems need a professional RFID reader or USRP to send RF signals at approximately 915 MHz so that they cannot be integrated into a smart home, whereas REHSENSE harvests RF energy from the Wi-Fi signals (*e.g.*, 2.4 GHz) radiated from Wi-Fi routers that are widely deployed in most indoor scenarios and also demonstrate the feasibility of being totally battery-free. Therefore, REHSENSE is much more practical and energy-efficient than RFID-based backscatter sensing systems.

5 RELATED WORKS

Wearable sensing. Wearable sensing techniques have been widely studied over the past few decades, which exploit sensor data collected from wearable devices to enable various sensing applications [41–50]. For instance, IMU-based systems utilize IMU sensors (*i.e.*, accelerometer, gyroscope, and magnetometer) equipped in mobile devices (*i.e.*, smartphone, smartwatch) to infer human activities [35], translate gesture-based sign language [51], and realizes automatic key generation for on-body communication [52]. Cao *et al.* utilize the built-in accelerometer and magnetometer of smart terminals to extract information representing user identity, achieving convenient and efficient authentication for heterogeneous IoT devices [53, 54]. Instead of requiring the user to wear sensor-based devices, REHSENSE introduces a novel non-intrusive sensing method, RF energy harvesting, and achieves fine-grained wireless sensing tasks with high effectiveness as well as low power consumption [55].

Wireless sensing. Wireless sensing has been widely studied because of its promising performance and contact-free manner [19, 56–76]. Most existing wireless sensing works [1, 2, 5, 7, 77] focus on extracting Wi-Fi CSI as the channel measurement because of its granularity and compatibility with COTS devices. Recent CSI-based sensing studies have formulated the theoretical description of the Fresnel diffraction sensing model and the results indicate good identification performance and generalization ability in respiration monitoring [8, 31], activity recognition [4], and gesture recognition [6]. However, almost all CSI-based sensing systems need to modify the transceivers and use power-intensive Wi-Fi NICs to capture wireless channel information. Furthermore, WiKI-Eye [78] shows the beamforming feedback information (BFI) could be exploited to infer user credentials such as smartphone passwords. Compared with these works, REHSENSE has demonstrated competitive human sensing performance without modifying the COTS

devices. In addition, our system requires much less energy consumption than a conventional CSI-based system, and the harvested RF energy can be reused to power other electronic components such as LED lights and Bluetooth modules.

6 CONCLUSION

In this paper, we present REHSENSE, a novel wireless sensing system based on RF energy harvesting. We address two major limitations of existing Wi-Fi based wireless sensing systems by using RF energy for the dual purpose of energy harvesting and sensing. We design and implement a prototype of REHSENSE and comprehensively evaluate its performance in three common human sensing tasks: respiration monitoring, human activity recognition, and hand gesture recognition. Experiments show that REHSENSE achieves high accuracy in these sensing tasks for different routers and environments. Comparison with a traditional Wi-Fi based sensing system shows that REHSENSE achieves comparable accuracy and good adaptation ability while reducing energy consumption significantly. Moreover, we demonstrate the feasibility of REHSENSE by integrating it into commodity IoT devices and implement a prototype to demonstrate the potential of battery-free sensing. We envision the wide deployment of REHSENSE when future smart IoT devices are equipped with RF energy harvesting techniques.

ACKNOWLEDGMENTS

We sincerely thank Prof. Haiming Jin for shepherding our paper and the anonymous reviewers for their constructive comments. This work was supported by Hong Kong RGC (Project No. CityU 21201420/11201422), the Innovation and Technology Commission of Hong Kong (Project No. PRP/037/23FX and MHP/072/23), NSF of Shandong Province (Project No. ZR2021LZH010), and NSF of Guangdong Province (Project No. 2414050001974). Any opinions, findings, and conclusions in this paper are those of the authors and not necessarily of the supported organizations.

REFERENCES

- [1] Xuefeng Liu, Jiamnong Cao, Shaojie Tang, Jiaqi Wen, and Peng Guo. Contactless respiration monitoring via off-the-shelf Wi-Fi devices. *IEEE Transactions on Mobile Computing*, 15(10):2466–2479, 2015.
- [2] Youwei Zeng, Dan Wu, Ruiyang Gao, Tao Gu, and Daqing Zhang. Fullbreath: Full human respiration detection exploiting complementary of CSI phase and amplitude of Wi-Fi signals. *Proceedings of ACM IMWUT*, 2(3):1–19, 2018.
- [3] Xuyu Wang, Chao Yang, and Shiwen Mao. On CSI-based vital sign monitoring using commodity Wi-Fi. *ACM Transactions on Computing for Healthcare*, 1(3):1–27, 2020.
- [4] Fusang Zhang, Kai Niu, Jie Xiong, Beihong Jin, Tao Gu, Yuhang Jiang, and Daqing Zhang. Towards a diffraction-based sensing approach on human activity recognition. *Proceedings of ACM IMWUT*, 3(1):1–25, 2019.
- [5] Wei Wang, Alex X Liu, Muhammad Shahzad, Kang Ling, and Sanglu Lu. Device-free human activity recognition using commercial Wi-Fi devices. *IEEE JSAC*, 35(5):1118–1131, 2017.
- [6] Ruiyang Gao, Wenwei Li, Yaxiong Xie, Enze Yi, Leye Wang, Dan Wu, and Daqing Zhang. Towards robust gesture recognition by characterizing the sensing quality of Wi-Fi signals. *Proceedings of ACM IMWUT*, 6(1):1–26, 2022.
- [7] Wenfeng He, Kaishun Wu, Yongpan Zou, and Zhong Ming. Wig: Wi-Fi-based gesture recognition system. In *Proceedings of ICCCN*, pages 1–7. IEEE, 2015.
- [8] Kai Niu, Fusang Zhang, Xuanzhi Wang, Qin Lv, Haitong Luo, and Daqing Zhang. Understanding Wi-Fi signal frequency features for position-independent gesture sensing. *IEEE Transactions on Mobile Computing*, 2021.
- [9] Daniel Halperin, Wenjun Hu, Anmol Sheth, and David Wetherall. Tool release: Gathering 802.11 n traces with channel state information. *Proceedings of the ACM SIGCOMM*, 41(1):53–53, 2011.
- [10] Yaxiong Xie, Zhenjiang Li, and Mo Li. Precise power delay profiling with commodity Wi-Fi. In *Proceedings of MobiCom*. ACM, 2015.
- [11] Daniel Halperin, Ben Greenstein, Anmol Sheth, and David Wetherall. Demystifying 802.11 n power consumption. In *Proceedings of HotPower*, page 1. USENIX Association, 2010.
- [12] Ki-Young Jang, Shuai Hao, Anmol Sheth, and Ramesh Govindan. Snooze: Energy management in 802.11 n wlans. In *Proceedings of the 7th Conference on Emerging Networking Experiments and Technologies*, pages 1–12, 2011.
- [13] Zhiping Jiang, Tom H Luan, Xincheng Ren, Dongtao Lv, Han Hao, Jing Wang, Kun Zhao, Wei Xi, Yueshen Xu, and Rui Li. Eliminating the barriers: Demystifying Wi-Fi baseband design and introducing the picoscenics Wi-Fi sensing platform. *IEEE Internet of Things Journal*, 9(6):4476–4496, 2021.
- [14] Nick Lavars. Scientists harvest Wi-Fi signals to power an led. <https://newatlas.com/electronics/small-chip-wi-fi-signals-power-led-light/>.
- [15] Marco Giordano and Michele Magno. A battery-free long-range wireless smart camera for face recognition. In *Proceedings of SenSys*, 2021.
- [16] Federico Villani, Philipp Mayer, and Michele Magno. Rf power transmission: Energy harvesting for self-sustaining miniaturized sensor nodes. In *Proceedings of SenSys*, pages 592–593, 2021.
- [17] Bryce Kellogg, Vamsi Talla, and Shyamnath Gollakota. Bringing gesture recognition to all devices. In *Proceedings of NSDI*, pages 303–316, 2014.
- [18] Yu Luo, Lina Pu, Guodong Wang, and Yanxiao Zhao. Rf energy harvesting wireless communications: Rf environment, device hardware and practical issues. *Sensors*, 19(13):3010, 2019.
- [19] Tao Ni, Yongliang Chen, Keqi Song, and Weitao Xu. A simple and fast human activity recognition system using radio frequency energy harvesting. In *Proceedings of ACM IMWUT*, pages 666–671, 2021.
- [20] Sangkil Kim, Rushi Vyas, Jo Bito, Kyriaki Niotaki, Ana Collado, Apostolos Georgiadis, and Manos M Tentzeris. Ambient rf energy-harvesting technologies for self-sustainable standalone wireless sensor platforms. *Proceedings of the IEEE*, 2014.
- [21] Manish Wadhwa, Min Song, Vinay Rali, and Sachin Shetty. The impact of antenna orientation on wireless sensor network performance. In *Proceedings of ICCSIT*, pages 143–147. IEEE, 2009.
- [22] Daqing Zhang, Hao Wang, and Dan Wu. Toward centimeter-scale human activity sensing with Wi-Fi signals. *Computer*, 50(1):48–57, 2017.
- [23] Hristo D Hristov. Fresnel zones in wireless links, zone plate lenses and antennas; artech house. *Inc.: Norwood, MA, USA*, 2000.
- [24] Daqing Zhang, Fusang Zhang, Dan Wu, Jie Xiong, and Kai Niu. Fresnel zone based theories for contactless sensing. In *Contactless Human Activity Analysis*, pages 145–164. Springer, 2021.
- [25] Jian Liu, Hongbo Liu, Yingying Chen, Yan Wang, and Chen Wang. Wireless sensing for human activity: A survey. *IEEE Communications Surveys & Tutorials*, 22(3):1629–1645, 2019.
- [26] Jianwen Luo, Kui Ying, and Jing Bai. Savitzky–golay smoothing and differentiation filter for even number data. *Signal Processing*, 2005.
- [27] Deepshikha Acharya, Asha Rani, Shivangi Agarwal, and Vijander Singh. Application of adaptive savitzky–golay filter for eeg signal processing. *Perspectives in science*, 8:677–679, 2016.
- [28] FLOWTIME. Flowtime biosensing meditation headband. <https://www.meetflowtime.com/>.
- [29] Hadeel Aboueidah, Nasma Abbas, Nadeen El-Nachar, Aya Al-Yousef, Mohammad Alhawari, Baker Mohammad, Hani Saleh, Tasneem Assaf, and Mohammed Ismail. Characterization of rf energy harvesting at 2.4 ghz. In *Proceedings of ICECS*, pages 446–449. IEEE, 2017.
- [30] Vamsi Talla, Bryce Kellogg, Shyamnath Gollakota, and Joshua R Smith. Battery-free cellphone. *Proceedings of the ACM on Interactive, Mobile, Wearable and Ubiquitous Technologies*, 1(2):1–20, 2017.
- [31] Fusang Zhang, Daqing Zhang, Jie Xiong, Hao Wang, Niu Kai, Beihong Jin, and Yuxiang Wang. From fresnel diffraction model to fine-grained human respiration sensing with commodity Wi-Fi devices. In *Proceedings of ACM IMWUT*, pages 1–23, 2018.
- [32] Ali Saffari, Mehrdad Hessar, Saman Naderiparizi, and Joshua R Smith. Battery-free wireless video streaming camera system. In *Proceedings of the IEEE International Conference on RFID*, pages 1–8. IEEE, 2019.
- [33] Mingmin Zhao, Tianhong Li, Mohammad Abu Alsheikh, Yonglong Tian, Hang Zhao, Antonio Torralba, and Dina Katabi. Through-wall human pose estimation using radio signals. In *Proceedings of CVPR*, pages 7356–7365, 2018.
- [34] Tianhong Li, Lijie Fan, Mingmin Zhao, Yingcheng Liu, and Dina Katabi. Making the invisible visible: Action recognition through walls and occlusions. In *Proceedings of ICCV*, pages 872–881, 2019.
- [35] Jennifer R Kwapisz, Gary M Weiss, and Samuel A Moore. Activity recognition using cell phone accelerometers. *ACM SigKDD Explorations Newsletter*, 12(2):74–82, 2011.
- [36] Omid Dehzangi and Vaishali Sahu. Imu-based robust human activity recognition using feature analysis, extraction, and reduction. In *Proceedings of the 24th International Conference on Pattern Recognition (ICPR)*, pages 1402–1407. IEEE, 2018.

- [37] Sara Khalifa, Guohao Lan, Mahbub Hassan, Aruna Seneviratne, and Sajal K Das. Harke: Human activity recognition from kinetic energy harvesting data in wearable devices. *IEEE Transactions on Mobile Computing*, 17(6):1353–1368, 2017.
- [38] Weitao Xu, Guohao Lan, Qi Lin, Sara Khalifa, Neil Bergmann, Mahbub Hassan, and Wen Hu. Keh-gait: Towards a mobile healthcare user authentication system by kinetic energy harvesting. In *Proceedings of NDSS*, 2017.
- [39] Xinyu Li, Yanyi Zhang, Ivan Marsic, Aleksandra Sarcevic, and Randall S Burd. Deep learning for rfid-based activity recognition. In *Proceedings of the 14th ACM Conference on Embedded Network Sensor Systems CD-ROM*, pages 164–175, 2016.
- [40] Han Ding, Jinsong Han, Longfei Shangguan, Wei Xi, Zhiping Jiang, Zheng Yang, Zimu Zhou, Panlong Yang, and Jizhong Zhao. A platform for free-weight exercise monitoring with passive tags. *IEEE Transactions on Mobile Computing*, 16(12):3279–3293, 2017.
- [41] Di Duan, Zehua Sun, Tao Ni, Shuaicheng Li, Xiaohua Jia, Weitao Xu, and Tianxing Li. F2key: Dynamically converting your face into a private key based on cots headphones for reliable voice interaction. In *Proceedings of the 22nd Annual International Conference on Mobile Systems, Applications and Services*, pages 127–140, 2024.
- [42] Tao Ni. Sensor security in virtual reality: Exploration and mitigation. In *Proceedings of the 22nd Annual International Conference on Mobile Systems, Applications and Services*, pages 758–759, 2024.
- [43] Ülkü Meteriz-Yıldırın, Necip Fazıl Yıldırın, and David Mohaisen. Sia: Smartwatch-enabled inference attacks on physical keyboards using acoustic signals. In *Proceedings of the 20th Workshop on Workshop on Privacy in the Electronic Society*, 2021.
- [44] Ülkü Meteriz-Yıldırın, Necip Fazıl Yıldırın, Amro Awad, and David Mohaisen. A keylogging inference attack on air-tapping keyboards in virtual environments. In *Proceedings of the IEEE Conference on Virtual Reality and 3D User Interfaces (VR)*, 2022.
- [45] Ülkü Meteriz-Yıldırın, Necip Fazıl Yıldırın, and David Mohaisen. Acoustictype: Smartwatch-enabled cross-device text entry method using keyboard acoustics. In *Proceedings of the CHI Conference on Human Factors in Computing Systems Extended Abstracts*, 2022.
- [46] David Mohaisen. Understanding the privacy dimension of wearables through machine learning-enabled inferences. In *Proceedings of the 2023 on Systems and Network Telemetry and Analytics*, pages 1–1, 2023.
- [47] Shengzhe Lyu, Yongliang Chen, Di Duan, Renqi Jia, and Weitao Xu. Earda: Towards accurate and data-efficient earable activity sensing. *arXiv preprint arXiv:2406.16943*, 2024.
- [48] Abdulaziz Alghamdi, Ali Alkinnoon, Ahod Alghuried, and David Mohaisen. xr-droid: A benchmark dataset for ar/vr and security applications. *IEEE Transactions on Dependable and Secure Computing*, 2024.
- [49] Xiping Sun, Jing Chen, Kun He, Zhixiang He, Ruiying Du, Yebo Feng, Qingchuan Zhao, and Cong Wu. Earpass: Secure and implicit call receiver authentication using ear acoustic sensing. *arXiv preprint arXiv:2404.15000*, 2024.
- [50] Weitao Xu, Yiran Shen, Neil Bergmann, and Wen Hu. Sensor-assisted multi-view face recognition system on smart glass. *IEEE Transactions on Mobile Computing*, 17(1):197–210, 2017.
- [51] Jiao Li, Yang Liu, Weitao Xu, and Zhenjiang Li. Gasla: Enhancing the applicability of sign language translation. In *Proceedings of IEEE INFOCOM*, pages 1249–1258. IEEE, 2022.
- [52] Weitao Xu, Girish Revadigar, Chengwen Luo, Neil Bergmann, and Wen Hu. Walkie-talkie: Motion-assisted automatic key generation for secure on-body device communication. In *Proceedings of the 15th ACM/IEEE IPSN*, pages 1–12. IEEE, 2016.
- [53] Hangcheng Cao, Daibo Liu, Hongbo Jiang, and Jun Luo. Magsign: Harnessing dynamic magnetism for user authentication on iot devices. *IEEE Transactions on Mobile Computing*, 23(1):597–611, 2024.
- [54] Hangcheng Cao, Hongbo Jiang, Daibo Liu, and Jie Xiong. Evidence in hand: Passive vibration response-based continuous user authentication. In *IEEE ICDCS*, pages 1020–1030, 2021.
- [55] Tao Ni, Zehua Sun, Mingda Han, Guohao Lan, Yaxiong Xie, Zhenjiang Li, Tao Gu, and Weitao Xu. Rehsense: Towards battery-free wireless sensing via radio frequency energy harvesting. In *Proceedings of the 25th International Symposium on Theory, Algorithmic Foundations, and Protocol Design for Mobile Networks and Mobile Computing*, 2024.
- [56] Tao Ni, Guohao Lan, Jia Wang, Qingchuan Zhao, and Weitao Xu. Eavesdropping mobile app activity via {Radio-Frequency} energy harvesting. In *32nd USENIX Security Symposium (USENIX Security 23)*, pages 3511–3528, 2023.
- [57] Tao Ni, Jianfeng Li, Xiaokuan Zhang, Chaoshun Zuo, Wubing Wang, Weitao Xu, Xiapu Luo, and Qingchuan Zhao. Exploiting contactless side channels in wireless charging power banks for user privacy inference via few-shot learning. In *Proceedings of the 29th Annual International Conference on Mobile Computing and Networking*, pages 1–15, 2023.
- [58] Tao Ni, Xiaokuan Zhang, and Qingchuan Zhao. Recovering fingerprints from in-display fingerprint sensors via electromagnetic side channel. In *Proceedings of the 2023 ACM SIGSAC Conference on Computer and Communications Security*, pages 253–267, 2023.
- [59] Tao Ni, Xiaokuan Zhang, Chaoshun Zuo, Jianfeng Li, Zhenyu Yan, Wubing Wang, Weitao Xu, Xiapu Luo, and Qingchuan Zhao. Uncovering user interactions on smartphones via contactless wireless charging side channels. In *2023 IEEE Symposium on Security and Privacy (SP)*, pages 3399–3415. IEEE, 2023.
- [60] Hanqing Guo, Nan Zhang, Wenjun Shi, Saeed AlQarni, and Shaoen Wu. Real time 3d indoor human image capturing based on fmcw radar. *arXiv preprint arXiv:1812.07099*, 2018.
- [61] Tao Ni, Yongliang Chen, Weitao Xu, Lei Xue, and Qingchuan Zhao. Xporter: A study of the multi-port charger security on privacy leakage and voice injection. In *Proceedings of the 29th Annual International Conference on Mobile Computing and Networking*, pages 1–15, 2023.
- [62] Shangyue Zhu, Junhong Xu, Hanqing Guo, Qiwei Liu, Shaoen Wu, and Honggang Wang. Indoor human activity recognition based on ambient radar with signal processing and machine learning. In *2018 IEEE international conference on communications (ICC)*, pages 1–6. IEEE, 2018.
- [63] Tao Ni, Qing Wang, and Gabriela Ferraro. Explore bilstm-crf-based models for open relation extraction. *arXiv preprint arXiv:2104.12333*, 2021.
- [64] Zehua Sun, Tao Ni, Huanqi Yang, Kai Liu, Yu Zhang, Tao Gu, and Weitao Xu. Flora: Energy-efficient, reliable, and beamforming-assisted over-the-air firmware update in lora networks. In *Proceedings of the 22nd International Conference on Information Processing in Sensor Networks*, pages 14–26, 2023.
- [65] Zehua Sun, Tao Ni, Huanqi Yang, Kai Liu, Yu Zhang, Tao Gu, and Weitao Xu. Flora+: Energy-efficient, reliable, beamforming-assisted, and secure over-the-air firmware update in lora networks. *ACM Transactions on Sensor Networks*, 20(3):1–28, 2024.
- [66] Zehua Sun, Tao Ni, Yongliang Chen, Di Duan, Kai Liu, and Weitao Xu. Rf-egg: An rf solution for fine-grained multi-target and multi-task egg incubation sensing. In *Proceedings of the 30th Annual International Conference on Mobile Computing and Networking*, pages 528–542, 2024.
- [67] Zehua Sun, Tao Ni, Huanqi Yang, Kai Liu, Yu Zhang, Tao Gu, and Weitao Xu. Demo abstract: A novel firmware update over-the-air system for lora networks. In *Proceedings of the 22nd International Conference on Information Processing in Sensor Networks*, pages 362–363, 2023.
- [68] Mingda Han, Huanqi Yang, Tao Ni, Di Duan, Mengzhe Ruan, Yongliang Chen, Jia Zhang, and Weitao Xu. mmsign: mmwave-based few-shot online handwritten signature verification. *ACM Transactions on Sensor Networks*, 20(4):1–31, 2024.
- [69] Keqi Song, Tao Ni, Linqi Song, and Weitao Xu. Emma: An accurate, efficient, and multi-modality strategy for autonomous vehicle angle prediction. *Intelligent and Converged Networks*, 4(1):41–49, 2023.
- [70] Keqi Song, Zimeng Zhu, Huanqi Yang, Tao Ni, and Weitao Xu. Mobilekey: A fast and robust key generation system for mobile devices. In *Adjunct Proceedings of the 2022 ACM International Joint Conference on Pervasive and Ubiquitous Computing and the 2022 ACM International Symposium on Wearable Computers*, pages 427–431, 2022.
- [71] Yongliang Chen, Tao Ni, Weitao Xu, and Tao Gu. Swipepass: Acoustic-based second-factor user authentication for smartphones. *Proceedings of the ACM on Interactive, Mobile, Wearable and Ubiquitous Technologies*, 6(3):1–25, 2022.
- [72] Rucheng Wu, Huanqi Yang, and Weitao Xu. Xsolar: A generative framework for solar-based human gesture sensing via wearable signals. In *Proceedings of the Workshop on Body-Centric Computing Systems*, pages 41–46, 2024.
- [73] Hangcheng Cao, Wenbin Huang, Guowen Xu, Xianhao Chen, Ziyang He, Jingyang Hu, Hongbo Jiang, Daibo Liu, Zhu Xiao, Hangcheng Cao, Yue Qi, Schahram Dustdar, and Jiangchuan Liu. Earsonar: An acoustic signal-based middle-ear effusion detection using earphones. In *2023 IEEE 43rd International Conference on Distributed Computing Systems (ICDCS)*, pages 225–235. IEEE, 2023.
- [74] Tiantian Liu, Ming Gao, Feng Lin, Chao Wang, Zhongjie Ba, Jinsong Han, Wenyao Xu, and Kui Ren. Wavoice: A noise-resistant multi-modal speech recognition system fusing mmwave and audio signals. In *Proceedings of the 19th ACM Conference on Embedded Networked Sensor Systems*, pages 97–110, 2021.
- [75] Tiantian Liu, Feng Lin, Chao Wang, Chenhan Xu, Xiaoyu Zhang, Zhengxiong Li, Wenyao Xu, Ming-Chun Huang, and Kui Ren. Wavoid: Robust and secure multi-modal user identification via mmwave-voice mechanism. In *Proceedings of the 36th Annual ACM Symposium on User Interface Software and Technology*, pages 1–15, 2023.
- [76] Xuyu Wang, Chao Yang, and Shiwen Mao. Phasebeat: Exploiting CSI phase data for vital sign monitoring with commodity Wi-Fi devices. In *Proceedings of ICDCS*, pages 1230–1239. IEEE, 2017.
- [77] Jingyang Hu, Hongbo Wang, Tianyue Zheng, Jingzhi Hu, Zhe Chen, Hongbo Jiang, and Jun Luo. Password-stealing without hacking: Wi-fi enabled practical keystroke eavesdropping. In *Proceedings of CCS*, pages 239–252, 2023.